Correlation of Mechanical Behaviors with Crystalline Phase and Related Cavitation in Isotactic Polypropylene

Ruihua Lv, Wenfei Xu, Bing Na, Junzhang Yan

Department of Materials Science and Engineering, East China Institute of Technology, Fuzhou 344000, People's Republic of China

Received 25 July 2007; accepted 27 December 2007
DOI 10.1002/app.27971
Published online 29 February 2008 in Wiley InterScience (www.interscience.wiley.com).

ABSTRACT: The β→α phase transformation during annealing of β-nucleated isotactic polypropylene (iPP) at 160°C for 1 h has been confirmed by differential scanning calorimetry and X-ray diffraction measurements. The α-crystals and related crystallinity in the annealed samples result in higher yield stress and volume dilatation, indicated by the true stress–strain and volume strain analysis, respectively. Meanwhile, higher volume dilatation can find its origin in the lower network modulus in the annealed samples. The increasing yield stress and volume strain, related to the crystalline phase (including crystal form and crystallinity), furthermore, should be responsible for the significant deterioration of the fracture toughness in the annealed samples determined by the essential work of fracture tests. © 2008 Wiley Periodicals, Inc. J Appl Polym Sci 108: 3185–3190, 2008

Key words: mechanical behaviors; crystalline phase; cavitation; isotactic polypropylene

INTRODUCTION

As an important semicrystalline polymer, the relationship between structure and mechanical properties in isotactic polypropylene (iPP) has been conducted extensively in the past.[1–10] The crystalline domain and the entangled amorphous network in iPP have different mechanical responses while subjected to the tensile deformation. Yield is dominated by the crystalline phase and can be formulated within the framework of crystal plasticity theory.[11] With proceeding of the strain, the mechanical response at large strain is mostly taken over by the entangled amorphous network that is represented by trapped chain entanglements as well as crystallites acting as physical crosslinks.[12] Like amorphous polymers,[13] moreover, the mechanical responses at large strain in iPP can be also described by neoHookean elasticity proposed by Harward.[14] Herein, crystallites serve as fillers to enhance the entangled amorphous network.[2,6] It is desired to note that the true stress–strain curves for extracting the network properties of entangled amorphous phase are generally based on the assumption of constant volume. However, upon tensile deformation macroscopic whitening can be inevitably induced in iPP because of the presence of negative pressure,[15–17] and it originates from noncohesive damage mechanisms, namely cavitation, at microscopic scale. Therefore, absence of volume dilatation may overestimate the effect of entangled amorphous network on mechanical responses at large strain in iPP. On the other hand, plastic flow and strain hardening ahead of notches play a vital role in the failure and toughness of iPP.[18] The toughness can be formulated by the intrinsic deformation parameters, namely yield stress and amorphous network modulus.[19] Increasing amorphous network modulus or decreasing yield stress is helpful for improvement of toughness. Besides, the cavitation ahead of notches can also affect the failure and toughness to some extent.[8]

Different molecular characteristics, such as number of branches, molecular weight, and type of comonomer, are usually adopted in achieving various structures.[7–9] It could lead to some controversial results with respect to the relationship between structure and mechanical behaviors. Concerning of the phase transformation of β-form crystals in iPP upon annealing at high temperature,[20,21] in this study, virgin and annealed β-iPP will be chosen to comparatively investigate the effect of crystalline phase and related cavitation on the mechanical behaviors.

EXPERIMENTAL

Materials and sample preparation

A commercial-grade iPP homopolymer, supplied by Dusanzi Petrochemical Corp., China, had a weight–

Correspondence to: B. Na (bingnash@163.com or bna@ecit.edu.cn).

Contract grant sponsor: National Natural Science Foundation of China; contract grant number: 20704006.
Contract grant sponsor: Natural Science Foundation of Jiangxi, China; contract grant number: 0650009.
Contract grant sponsor: Doctoral Special Foundation from ECIT.

© 2008 Wiley Periodicals, Inc.
WILEY InterScience® DISCOVER SOMETHING GREAT

average molecular weight M_w 2.5 × 10^5 g/mol and M_w/M_n is 3.1 It was modified with a selective β-nucleation agent, N, N′- dicyclohexylnaphthalene-2, 6-dicarboxamide, in a concentration of 0.3 wt % by melt blending conducted in a TSSJ-2S corotating twin-screw extruder. The temperature of the extruder was maintained at 160–210°C from hopper to die, respectively, and the screw speed was about 110 rpm/min. Subsequently, the dried pellets were placed in a hot press with a temperature of 200°C and a pressure of 2 MPa to prepare the samples for mechanical tests. The samples were quickly transferred to a cold press for rapid cooling under a slight pressure after being held for 5 min in the press. The thickness of the samples was about 0.5 mm. The samples subjected to the above procedure were referred to virgin ones. The virgin ones were placed again in the hot press preset at 160°C for 1 h and then quenched to room temperature in a cold press under a slight pressure to obtain the annealed samples.

Differential scanning calorimetry

The thermal analysis of the samples was conducted using a NETZSCH DSC 204, indium calibrated. Melting endotherms were obtained with 6–8 mg of sample at a heating rate of 10°C/min in a nitrogen atmosphere. The enthalpy of melting of 100% crystalline α- and β-iPP is 177 J/g and 168.5 J/g, respectively.[22]

X-ray diffraction measurements

Wide-angle X-ray diffraction (XRD) was measured on an X-ray diffractometer equipped with an X-ray generator and a goniometer. The X-rays were generated at 35 kV and 60 mA and the wavelength of the monochromated X-ray from CuK_α radiation was 0.154 nm.

Video-aid tensile tests

Uniaxial tensile tests were performed on a dog-bone sample (4 mm width × 6 mm gauge length) using a universal testing machine at room temperature. A CCD camera (1280 pixel × 1024 pixel) equipped with a tunable magnification lens was adopted to obtain true stress and true strain. Its image resolution was 80-pixels/mm. Several grids, one of which had a space of 0.2 mm and 3 mm along the axial and transverse direction of the dog-bone sample, respectively, were preprinted on the sample with ink. The grid deformed first was monitored by the CCD camera and its space change in the axial and transverse direction was simultaneously recorded during tensile stretching. The value of true stress, true strain, and volume strain can be deduced with knowledge of load and transient space, which has been well demonstrated elsewhere.[23]

Essential work of fracture tests

Essential work of fracture (EWF) tests were conducted by tensile deformation of the deeply double edge-notched strips with a gauge length of 10 mm and a width of 15 mm. Initial notches were made perpendicularly to the tensile direction with a fresh razor blade. The ligament lengths of specimens were varied between 2.5 and 5 mm to meet the demands of both plane stress and free constraint of boundary. Detail descriptions as to the EWF measurements can be found elsewhere.[24–26] The ligament lengths were accurately measured at the initial deformation stage with aid of the CCD camera mentioned earlier. With real time registration of images, it was possible to directly correlate the two-dimensional deformation states to the characteristic points of the load-displacement curve. The load-displacement curves were recorded during deformation, and from which the absorbed energy was calculated.

RESULTS AND DISCUSSION

Properties of the crystalline phase

Figure 1 is the heating traces of the virgin and annealed sample, respectively, at a heating rate of 10°C/min. The endothermic peak below 160°C in the virgin sample results from the melting of β-form crystals, and the one above 160°C can be ascribed to the melting of recrystallized α-form crystals.[20–22] As for the annealed sample, only the melting trace corresponding to α-form crystals is presented, indicating that annealing at 160°C for 1 h is enough to alter

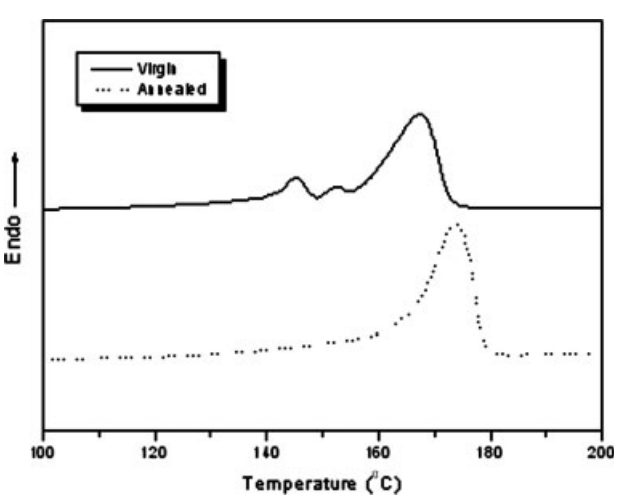

Figure 1 Heating traces of both virgin and annealed samples at a rate of 10°C/min.

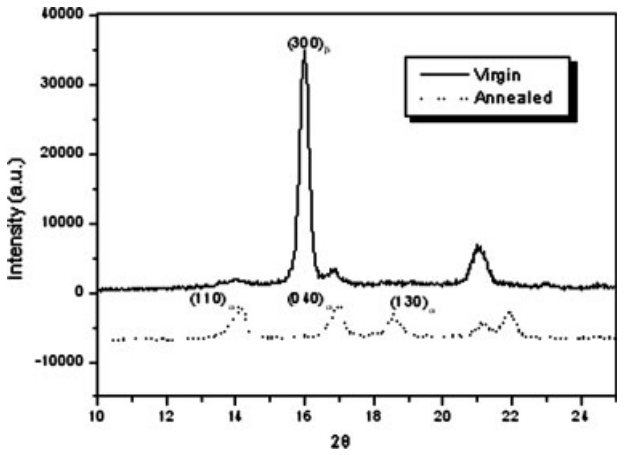

Figure 2 XRD patterns recorded from the virgin and annealed sample, respectively. Note that only α-form crystals are presented in the annealed sample.

the crystalline phase. The crystal transformation during annealing can be further confirmed by the XRD results shown in Figure 2. The reflection of (300) crystal plane in the virgin sample, a characteristic of β-form crystals, is entirely absent in the annealed one, suggesting β→α phase transformation during annealing. In addition, the calculated crystallinity is 0.35 and 0.52 for the virgin and annealed sample, respectively.

Deformation behaviors and volume strain

Figure 3 is the true stress strain curves recorded from both virgin and annealed samples at a crosshead speed of 2 mm/min. The yield stress is 27.5 and 40.0 MPa for the virgin and annealed sample, respectively, which is consistent with the properties of crystalline phase (as evidenced by DSC and XRD results). Plastic flow becomes pronounced with increasing of strain after yield, and is different for the virgin and annealed sample. Steeper increasing of stress with strain is presented in the virgin sample. The flow stress exerted by the deformed sample can be divided into two parts: one is strain rate dependent and borne by a crystalline phase, and the other is strain dependent and consumed by a crystallite-enhanced amorphous network.[2,6,14,27,28] Therefore, the total flow stress can be expressed as,

$$\sigma = \sigma_C(\varepsilon) + \sigma_A(\varepsilon) \quad (1)$$

Moreover, the stress consumed by the crystallite-enhanced amorphous network can be formulated by the neoHookean rule,[14]

$$\sigma_A(\varepsilon) = G(\exp(2\varepsilon) - \exp(-\varepsilon)) \quad (2)$$

where G is the shear modulus. Fitting is made to the data of the virgin and annealed sample, respectively, with $\sigma_C(\varepsilon)$ and G as adjustable parameters. Such treatments, illustrated by the dot lines in the Figure 3, yield the value of $\sigma_C(\varepsilon)$ = 31.7 MPa and G = 2.5 MPa for the virgin sample, and $\sigma_C(\varepsilon)$ = 37.1 MPa and G = 1.0 MPa for the annealed sample, respectively. The values of $\sigma_C(\varepsilon)$ seem reasonable and are consistent with the properties of crystalline phase. However, much lower apparent network modulus is presented in the annealed sample.

Figure 4 is the evolution of volume strain with axial strain under stretching in the virgin and annealed sample, respectively. Volume dilatation begins around yield point and increases significantly with strain. Moreover, more severe volume dilatation is presented in the annealed sample, while com-

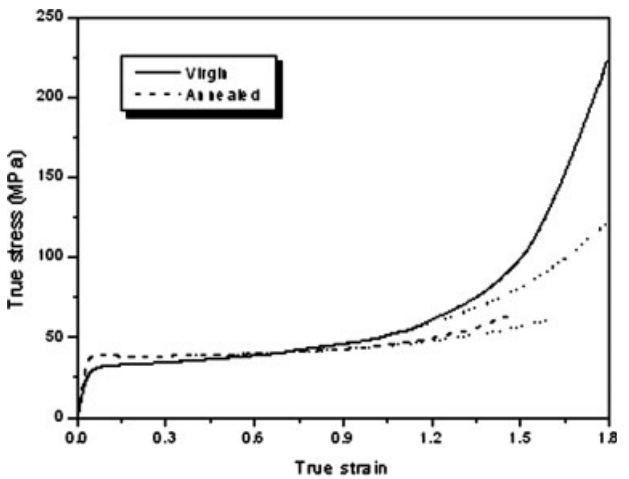

Figure 3 True stress–strain curve recorded from the virgin and annealed sample, respectively, at a crosshead speed of 2 mm/min. The dot lines are the fitting results based on eqs. (1) and (2) (see text).

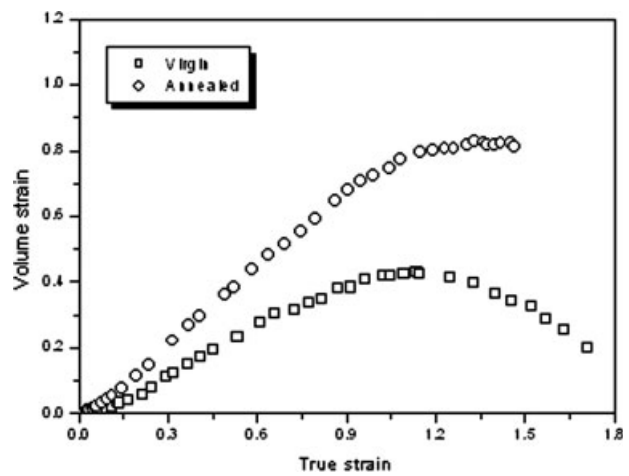

Figure 4 Evolution of the volume strain with axial strain under stretching in the virgin and annealed sample, respectively, at a crosshead speed of 2 mm/min.

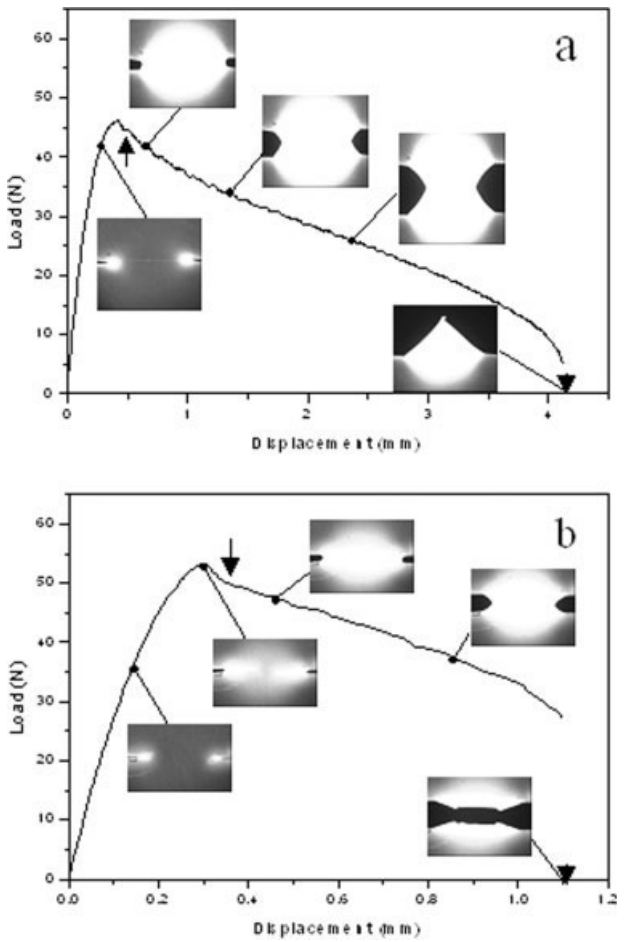

Figure 5 Correlation of two-dimensional states to the stress–displacement curves of the virgin (a) and annealed (b) sample, respectively, with a ligament length of 3.4 mm at a crosshead speed of 2 mm/min. Note that the arrows denote the onset of yield and crack propagation.

pared with that of the virgin one. Note that the decreasing of volume strain at large strain may result from the healing of voids due to reorientation of molecular chains.[29] It is well known that the volume dilatation under tensile deformation in semicrystalline polymers is mostly related to the nucleation and propagation of voids.[30] As argued by Pawlak and Galeski,[15] the formation of voids in tension results from the stress-dependent negative pressure. Increasing yield stress, related to the crystal form and crystallinity, can promote the negative pressure and thus volume dilatation. The α-crystal accompanied by higher crystallinity in the annealed samples is apparently the origin of higher volume dilatation. As to the same α-form, furthermore, lamellar thickness and related crystallinity is another factor affecting the volume dilatation. Thinner lamellae (indicated by lower melting point) with lower yield stress correspond to lower volume dilatation, which has been demonstrated in the quenched non-nucleated samples with α-crystals.[23] On the basis of the crystalline phase dependent volume dilatation, furthermore, it can be deduced that severer cavitation should be responsible for lower network modulus in the annealed sample shown in Figure 3 due to microporosity.

Failure and toughness

Figure 5 shows the deformation states of both virgin and annealed samples with a ligament length of 3.4 mm while subjected to tensile deformation at a crosshead speed of 2 mm/min. Apparently, yield is first initiated from the notches due to the stress concentration and thus stress-whitening zones are formed ahead of notches. Stress-whitening zones begin to grow from both sides and then merge into each other with increasing of elongation. Crack propagation sets in until the ultimate fracture of samples after total yield of whole ligament. Semibrittle fracture occurs in the annealed sample, whereas ductile one is present in the virgin sample. With real time registration of ligament width, moreover, the relation of crack growth versus time can be determined. Figure 6 is, for example, such plots derived from the virgin and annealed sample with a ligament length of 3.4 mm. Consistent with the results of two-dimensional deformation state, there are two distinct zones during the whole tensile deformation. In the first zone no crack grows, followed by stable crack propagation in the second zone (indicated by the arrows in Fig. 6). Note that increasing crack propagation at late stage in the annealed sample is related to its semibrittle fracture behavior. The crack growth rate is 0.014 and 0.024 mm/s for the virgin and annealed sample, respectively. Crack growth rate depends on the competition between network modulus and cohesive strength from the view of

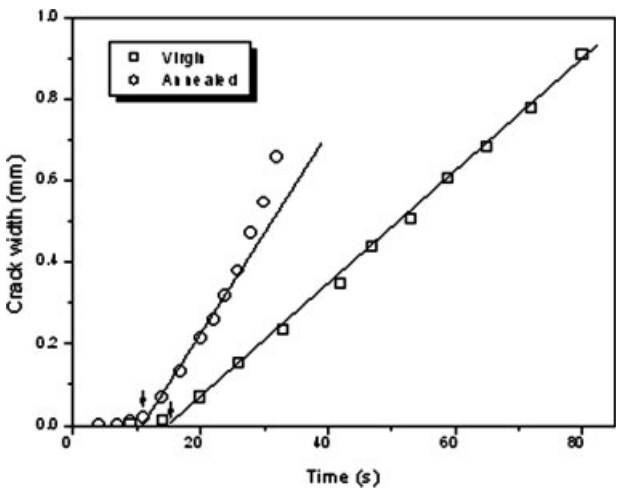

Figure 6 Plots of the crack width versus time for both virgin and annealed samples with a ligament length of 3.4 mm at a crosshead speed of 2 mm/min.

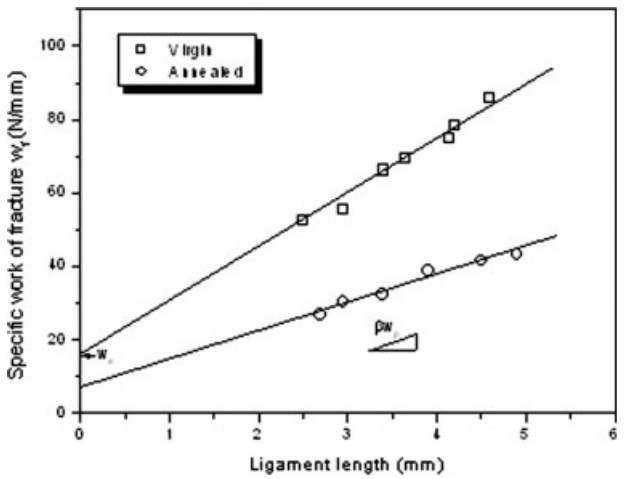

Figure 7 Plots of specific work of fracture βw_p as a function of the ligament length for both virgin and annealed samples with deeply double edge notches at a crosshead speed of 2 mm/min. Its interception at zero ligament length and its slope would give the specific EWF w_e, and the specific nonessential work of fracture βw_p, respectively.

fracture mechanics.[31] A crack will propagate when the network modulus exceeds the cohesive strength. Therefore, lower cohesive strength in the annealed sample, resulted from void formation, should be responsible for more severe crack propagation and thus semibrittle fracture is brought out.

Figure 7 is the plots of total energy dissipated on per unit area of ligament w_f versus ligament length for both virgin and annealed samples. As for the same ligament, the total energy dissipated on per unit area of ligament w_f is higher in the virgin sample. The deduced specific EWF w_e is 15.9 and 7.4 N/mm for the virgin and annealed sample, respectively. Note that the value of w_e for the quenched non-nucleated samples with thinner α-crystals is 8.2 N/mm, which is higher than that of annealed samples with thicker α-crystals in this case. Numerous studies have suggested that fracture toughness of iPP is related to the yield strength and craze strength or network modulus.[7,8] Increasing yield strength and/or decreasing network modulus from the volume dilatation, related to the crystal form and crystallinity, can reduce the fracture toughness, which is the origin of lower toughness in the annealed samples. The reason lies in that the deformation is confined in the notched zone during fracture tests due to stress concentration. Fracture toughness can be improved when the strength of the deformed material in the notched zone is high enough to induce the deformation of remained part in the surrounding zone of fracture plane. In addition to different crystal forms, the above principle is also applicable for the samples with the same α-crystals while comparing the fracture toughness of quenched non-nucleated samples (8.2 N/mm) with thinner lamellae and annealed ones with thicker lamellae in this case (7.4 N/mm). Therefore, it can be deduced that the fracture toughness is dominated by the properties of crystalline phase (including crystal form, lamellar thickness, and crystallinity) and related cavitation. The other stated argument is that formation of void can convert plane strain state to the plane stress one and thus improves the toughness.[8] In this case, however, void induced toughening is absent, when the toughness of annealed sample with higher volume dilatation is taken into account. In our viewpoint, the effect of cavitation on the toughness is two-folds: one is to induce conversion of stress state and thus promote shear yield; the other is to deteriorate the material due to decreasing of solid fraction. Therefore, toughness can be decreased when the latter prevails, which is the fact for the annealed sample.

CONCLUSIONS

Tensile deformation of both β-iPP and its annealed counterpart demonstrates that the yield behavior, plastic flow, and volume dilatation are dominated by the properties of the crystalline phase including crystal form and crystallinity. The α-crystal accompanied by higher crystallinity in the annealed samples corresponds to higher volume dilatation and thus lower network modulus. The fracture toughness, dependent of the yield stress, network modulus, and cavitation, can be well correlated with the properties of the crystalline phase.

References

1. Schrauwen, B. A. G.; Janssen, R. P. M.; Govaert, L. E.; Meijer, H. E. H. Macromolecules 2004, 37, 6069.
2. Song, Y.; Nemoto, N. Polymer 2005, 46, 6522.
3. Koike, Y.; Cakmak, M. Polymer 2003, 44, 4249.
4. Ferrer-Balas, D.; Maspoch, M. L.; Martinez, A. B.; Santana, O. O. Polymer 2001, 42, 1697.
5. Pluta, M.; Bartczak, Z.; Galeski, A. Polymer 2000, 41, 2271.
6. Song, Y.; Nemoto, N. Polymer 2006, 47, 489.
7. Ishikawa, M.; Ushui, K.; Kondo, Y.; Hatada, K.; Gima, S. Polymer 1996, 37, 5375.
8. Sugimoto, M.; Ishikawa, M.; Hatada, K. Polymer 1995, 36, 3675.
9. Ouederni, M.; Phillips, P. J. J Polym Sci Part B: Polym Phys 1995, 33, 1313.
10. Van der Wal, A.; Mulder, J. J.; Gaymans, R. J. Polymer 1998, 39, 5477.
11. Kristiansen, M.; Tervoort, T.; Smith, P.; Goossens, H. Macromolecules 2005, 38, 10461.
12. G'Sell, C.; Hiver, J. M.; Dahouin, A.; Souahi, A. J Mater Sci 1992, 27, 5031.
13. Ho, J.; Govaert, L.; Utz, M. Macromolecules 2003, 36, 7398.
14. Haward, R. N. Macromolecules 1993, 26, 5860.
15. Pawlak, A.; Galeski, A. Macromolecules 2005, 38, 9688.
16. Duffo, P.; Monasse, B.; Haudin, J. M.; G'Sell, C.; Dahoun, A. J Mater Sci 1995, 30, 701.

17. Li, J. X.; Cheung, W. L.; Chan, C. M. Polymer 1999, 40, 2089.
18. Galeski, A. Prog Polym Sci 2003, 28, 1643.
19. Na, B.; Lv, R. H. J Polym Sci Part B: Polym Phys 2006, 44, 2880.
20. Kotek, J.; Kelnar, I.; Baldrian, J.; Raab, M. Eur Polym Mater 2004, 40, 2731.
21. Marigo, A.; Marega, C.; Causin, V.; Ferrari, P. J Appl Polym Sci 2004, 91, 1008.
22. Lezak, E.; Bartczak, Z.; Galeski, A. Polymer 2006, 47, 8562.
23. Na, B.; Lv, R. H. J Appl Polym Sci 2007, 105, 3274.
24. Wu, J.; Mai, Y. W. Polym Eng Sci 1996, 36, 2275.
25. Lach, R.; Schneider, K.; Weidisch, R.; Janke, A.; Knoll, K. Eur Polym Mater 2005, 41, 383.
26. Karger-Kocsis, J.; Czigany, T.; Moskala, E. J. Polymer 1998, 39, 3939.
27. Hong, K.; Rastogi, A.; Strobl, G. Macromolecules 2004, 37, 10165.
28. Lin, L.; Argon, A. J Mater Sci 1994, 29, 294.
29. Fang, Q. Z.; Wang, T. J.; Li, H. M. Polymer 2006, 47, 5174.
30. Addiego, F.; Dahoun, A.; G'Sell, C.; Hiver, J. M. Polymer 2006, 47, 4387.
31. Hui, C. Y.; Jagota, A.; Bennison, S. J.; Londono, J. D. Proc R Soc Lond Ser A 2003, 459, 1489.